Deiodinase knockdown affects zebrafish eye development at the level of gene expression, morphology and function

Deiodinase knockdown affects zebrafish eye development at the level of gene expression, morphology and function.

Anne M. Houbrechts[1*], Lucia Vergauwen[2*], Enise Bagci[2,3], Jolien Van houcke[1], Marjolein Heijlen[1], Bernard Kulemeka[4], David R. Hyde[4], Dries Knapen[2], Veerle M. Darras[1]

[1] Laboratory of Comparative Endocrinology, Department of Biology, Division of Animal Physiology and Neurobiology, KU Leuven, 3000 Leuven, Belgium

[2] Zebrafishlab, Veterinary Physiology and Biochemistry, Department of Veterinary Sciences, University of Antwerp, Universiteitsplein 1, 2610 Wilrijk, Belgium

[3] Systemic Physiological & Ecotoxicological Research, Department of Biology, University of Antwerp, Universiteitsplein 1, 2610 Wilrijk, Belgium

[4] Department of Biological Sciences and Center for Zebrafish Research, University of Notre Dame, Notre Dame, Indiana, USA.

* both authors contributed equally to this work

Corresponding author: veerle.darras@bio.kuleuven.be

Abbreviations

D: deiodinases, D1D2MO: morpholino knockdown of D1 and D2, D3bMO: morpholino knockdown of D3b, dpf: days post fertilization, hpf: hours post fertilization, KD: knockdown, MO: morpholino, OKR: optokinetic response, RES: relative eye surface, SCMO: standard control morpholino, WIK: Wild Indian Karyotype

ABSTRACT

Retinal development in vertebrates relies extensively on thyroid hormones. Their local availability is tightly controlled by several regulators, including deiodinases (Ds). Here we used morpholino technology to explore the roles of Ds during eye development in zebrafish. Transcriptome analysis at 3 days post fertilization (dpf) revealed a pronounced effect of knockdown of both T_4-activating Ds (D1D2MO) or knockdown of T_3-inactivating D3 (D3bMO) on phototransduction and retinoid recycling. This was accompanied by morphological defects (studied from 1 to 7 dpf) including reduced eye size, disturbed retinal lamination and strong reduction in rods and all four cone types. Defects were more prominent and persistent in D3-deficient fish. Finally, D3-deficient zebrafish larvae had disrupted visual function at 4 dpf and were less sensitive to a light stimulus at 5 dpf. These data demonstrate the importance of TH-activating and -inactivating Ds for correct zebrafish eye development, and point to D3b as a central player.

KEYWORDS: thyroid hormone; deiodinase; morpholino knockdown; zebrafish; development; retina

1. INTRODUCTION

It is a well-known fact that thyroid hormones (THs) and TH receptors (TRs) are of crucial importance during vertebrate eye development (Gamborino et al, 2001; Havis et al, 2006; Kelley et al, 1995). The best studied part of the eye is the retina. Its structure is well conserved among vertebrates and is composed of three distinct nuclear layers, separated by two plexiform layers (Dowling, 1987). The photoreceptors (rods and cones) reside in the outer

nuclear layer. Their development is highly dependent on THs, as has been proven extensively in mammals and birds (Fischer et al, 2011; Ma et al, 2014; Ng et al, 2001; Roberts et al, 2006). Data are also available from fish and amphibians where photoreceptor development has mostly been studied in relation to TH-induced metamorphosis. In the African clawed frog (*Xenopus laevis*) for instance, asymmetrical growth of the retina during metamorphosis has been linked to a local difference in TH concentrations and hence a difference in cell proliferation in the ventral and dorsal part (Marsh-Armstrong et al, 1999). Moreover, in fish such as the winter flounder, increasing levels of TH during the progress of metamorphosis are required to generate a new complement of photoreceptors. Additionally, the photoreceptor specification and differentiation appears to be TH-dependent (Mader & Cameron, 2004; Mader & Cameron, 2006). During smoltification in salmonid fish THs lead to degeneration of ultraviolet sensitive cones via programmed cell death (Allison et al, 2006).

Although 3,5,3'-triiodothyronine (T_3) is most often the central player in TH-dependent regulation of development, this hormone is only produced in limited amounts by the thyroid gland, which mainly releases the prohormone 3,5,3',5'-tetraiodothyronine or thyroxin (T_4). The majority of T_3 is formed in the periphery by iodothyronine deiodinases. These enzymes catalyze the removal of iodine atoms from THs, thereby contributing to the regulation of their bioavailability in the cell. Deiodinases can be divided into three types: D1, D2 and D3, encoded by *dio1*, *dio2* and *dio3* respectively. The major activating deiodinase in fish is D2 which efficiently catalyzes outer ring deiodination of T_4 into the receptor-active T_3; D1 also contributes but only to a minor extent. T_3 can be inactivated into 3,3'-diiodothyronine (T_2) by inner ring deiodination, a reaction catalyzed by the major inactivating enzyme D3 (Bianco & Kim, 2006; Germain et al, 2009; Guo et al, 2014).

The best method to decipher deiodinase function is by means of deficiency models. The mouse was the first vertebrate species where this was possible by the creation of deiodinase

knockout lines. From D3-null mice we learned that the D3 enzyme is crucial for retinal cone receptor survival and maturation by protecting these cells from an excess of T_3 (Ng et al, 2010). Another research group substantiated these results by showing that stimulation of TH signaling promotes cone and rod photoreceptor death, while the opposite, suppression of TH signaling, preserves cone photoreceptors in degenerating adult mouse retinas (Ma et al, 2014). Kelley and colleagues (1995) on the other hand demonstrated that low doses of T_3 are essential for precursor cells to differentiate into cone photoreceptors *in vitro* (Kelley et al, 1995).

Another model species is the zebrafish, in which deiodinase deficiency can be induced by antisense morpholino knockdown (KD) (Heijlen et al, 2014; Walpita et al, 2010). We therefore used this approach to further investigate the role of deiodinases in vertebrate eye and retinal development. Zebrafish eye development starts around 12 hours post fertilization (hpf) (Bibliowicz & Gross, 2009; Dahm & Geisler, 2006). The different layers of the retina can be distinguished from 60 hpf onwards (Malicki et al, 1996) and around 4 days post fertilization (dpf), zebrafish sight is functional, as shown for instance by the start of the optokinetic response (Brockerhoff, 2006). Zebrafish possess five kinds of photoreceptors, each with a peak sensitivity to a specific wavelength of light: one type of rod photoreceptor and four types of cone photoreceptors (Ebrey & Koutalos, 2001; Vihtelic et al, 1999).

Recent analysis of the head transcriptome in zebrafish revealed a striking impact of deiodinase KD on the expression of genes related to the eye, showing a high number of downregulated genes (Bagci et al, 2015). Following KD of the activating or the inactivating deiodination pathway, the affected transcripts were mainly related to eye development and phototransduction. This was the motivation for the present study, which attempts to link changes in the transcriptome to effects at the morphological and functional level.

2. MATERIALS AND METHODS

2.1 Animals

The wild-type zebrafish strain Wild-Indian Karyotype (WIK) was housed in community tanks at 28 ± 1°C under a light/dark regime of 14/10 h. The tanks contained reconstituted fresh water (OECD 203 annex 2 (ISO-6341-1982), 1992: 290 mg/l $CaCl_2 \cdot 2H_2O$, 120 mg/l $MgSO_4 \cdot 7H_2O$, 60 mg/l $NaHCO_3$ and 6 mg/l KCl) and each tank was provided with a mechanic filter. The fish were fed ad libitum twice a day: in the morning they received formulated feed (Dr. Bassleer Biofish Food, Telgte, Germany) and in the evening *Artemia salina* larvae (cysts from Ocean Nutrition Europe, Essen, Belgium). Zebrafish eggs were collected 30 minutes after natural group spawning and rinsed with system water to remove contaminants. Embryos/larvae were reared in 0.3x Danieau's medium (17 mM NaCl, 2 mM KCl, 0.12 mM $MgSO_4$, 1.8 mM $Ca(NO_3)_2$ and 1.5 mM HEPES, pH 7.6) (CSH Protocols, 2011) in Petri dishes (PS, 90 x 16.2 mm, MLS NV, Belgium) with 40 animals per condition per dish and all conditions were co-incubated at 28 ± 0.5°C in the dark. All animal experiments were approved by the Institutional Ethical Committee of the KU Leuven (P102/2012 and P239/2013) and executed in strict accordance with the European Council Directive (2010/63/EC).

2.2 Microinjection

KD of either the TH-activating or TH-inactivating pathway was accomplished by means of antisense morpholino oligonucleotides (MOs), designed and obtained from Gene Tools, LLC (Philomath, OR, USA). All MOs used were translation blocking. To knock down both types of peripheral T_4 to T_3 conversion we used a combination of a *dio1*-specific MO (D1MO: 5'-AAATCCCACTGCGGACCCCATCGTG-3') and a *dio2*-specific MO (D2MO: 5'-TCCACACTAAGCAAGCCCATTTCGC-3') as previously described by our group (Walpita

et al, 2010). As a preliminary test we checked the effect of injection of 0.4 mM D1D2MO (0.2 mM D1MO + 0.2 mM D2MO) on outer ring deiodination in larvae of 72 hpf and found a more than 90% reduction of activity at both low and high substrate concentrations, reflecting D2 and D1 activity respectively. For the inactivating pathway, we focused on the D3b paralog, encoded by *dio3b*. Although zebrafish possess two *dio3* paralogs, D3b is highly predominant over D3a (Guo et al, 2014; Heijlen et al, 2014). We previously showed that injection of 0.4 mM of the same D3bMO (5'-CTGCGGAGCCCTGCAGCATCTCCAT-3') resulted in a 96% reduction of D3 enzyme activity at 72 hpf (Heijlen et al, 2014).

As a negative control, 0.4 mM of a standard control MO (SCMO: 5'-CCTCTTACCTCAGTTACAATTTATA-3', recommended by Gene Tools) was used in all experiments. This MO is directed against a human β-globin intron mutation and represents a widely used control for toxicity and off-target effects. For microinjections, a FemtoJet microinjector (Eppendorf) and a M3301 micromanipulator (World Precision Instruments, UK) were used. Injection needles were prepared from thin-wall capillaries with the PN-30 needle puller (Narishige, Japan). A volume of 2 nl translation blocking MO or SCMO was injected into the yolk of 2-4 cell stage embryos, resulting in a final dose of 6.6 ng of MO per embryo. Embryos that did not reach a normal blastula stage three hours after injection were removed from the dish. For the rescue experiments, 6.6 ng D3bMO was co-injected with 225 pg human *DIO3* mRNA (synthesized with the mMESSAGE mMACHINE T7 kit, Ambion) during the 2-cell stage, as described before (Heijlen et al, 2014).

Table 1 lists the number of animals and batches used in every experiment. Except for the rod and cone (3 stages) photoreceptor counting, all morphological and functional analyses were repeated on at least 2 different batches, each of them obtained from a single group spawning.

2.3 Transcriptome analysis by microarray

143 The complete transcriptome analysis was described in detail in Bagci et al. (2015). For each
144 condition, 40 embryos were reared together in a Petri dish. Using a stereomicroscope (M4A,
145 Wild Heerbruggbino) and a pair of #55 Dumont forceps (Fine Tools, Berlin), the heads
146 (including brain, sacculi/otolith and jaw parts) of 72 hpf-old larvae were manually dissected
147 in ice-cold RNAse-free water. Four biological replicates of 20 heads of each KD condition
148 (D1D2MO, D3bMO) and control condition (SCMO) were collected. Total RNA was
149 extracted, and linearly amplified and labelled using the Low Input Quick Amplification
150 Labelling Kit (LIQA, Agilent Technologies, Santa Clara, CA, USA). Each cRNA sample was
151 labelled once with Cy3-CTP and once with Cy5-CTP. These samples were hybridized to
152 Agilent's Zebrafish Gene Expression Microarray V3 in a 4x44k format using an A-optimal
153 design. Microarrays were washed, scanned (Genepix 4100A confocal scanner, Axon
154 Instruments, Union City, CA, USA) and features were extracted using the Genepix Pro
155 software 6.1 (Axon Instruments). After background correction and normalization,
156 significantly differentially expressed transcripts (false discovery rate < 0.05, |log2FC| > 0.585)
157 were identified using the R package Limma (Smyth, 2004) by contrasting KD conditions
158 against SCMO. Clustering, GO analysis and KEGG pathway analysis were used to identify
159 affected biological processes. In the current manuscript, we performed an in-depth pathway
160 analysis of all differentially expressed transcripts related to eye structure and function.

161 **2.4 Validation by quantitative PCR**

162 In order to validate the microarray results on transcripts related to eye structure and function
163 and confirm their eye-specific differential expression, we performed quantitative PCR (Q-
164 PCR), on RNA isolated from eyes of SCMO, D1D2MO and D3bMO injected larvae of 72
165 hpf. The eyes were manually dissected after placing the larvae in ice-cold RNAse-free water.
166 First, the head was separated from the body using a pair of #55 Dumont forceps (Fine Tools,
167 Berlin). Next, the head was pinned down so that the brain and skull fragments could be

168 removed. In total 40 eyes were pooled per replicate and immediately snap frozen on dry ice.
169 The samples were kept at -80°C until processing for RNA extraction.

170 RNA was extracted from four biological replicates for each condition using the Nucleospin®
171 RNA isolation kit (Macherey-Nagel, Düren, Germany) according to the manufacturer's
172 instructions. This includes a DNAse treatment. RNA purity and integrity were confirmed
173 using a NanoDrop spectrophotometer (NanoDrop Technologies, Montchanin, DE, USA) and
174 a BioAnalyzer (Agilent Technologies, Diegem, Belgium). cDNA was constructed using a
175 Revertaid H Minus First Strand cDNA Synthesis Kit (Thermo Fischer Scientific, Waltham,
176 MA, USA) according to the manufacturer's instructions, with random hexamer primers.

177 Q-PCR reactions were performed in an MX3005P (Agilent Technologies) using the Brilliant
178 II SYBR® Green Q-PCR Master Mix (Agilent Technologies) according to the manufacturer's
179 instructions. Thermal cycling profiles were: an initial denaturation period of 10 min at 95°C,
180 followed by 40 cycles of 20 s at 95°C, 40 s at 58°C and 50 s at 72°C. Melting curves were
181 analysed to confirm specific amplification. Based on measurements in all samples, *eef1a1l1*
182 and *actb1* were selected out of five potential reference genes, using a set of Excel macros,
183 geNorm (Vandesompele et al., 2002). Primers are listed in supplementary Table S1. All but
184 two primer sets have been previously published. These two primer sets were developed using
185 IDT primer design (Integrated DNA Technologies, Coralville, IA, USA). Fold changes were
186 calculated against SCMO, and normalized with the geometric mean of the two reference
187 genes, using the delta-delta-Ct method (Pfaffl et al., 2001). In each run, primer efficiencies
188 were determined on a dilution series of a sample containing aliquots of all test samples and
189 used in the calculations. Transcript levels were expressed as log2 fold change relative to the
190 average of the four SCMO biological replicates, such that they are directly comparable to the
191 microarray results (Supplementary figure S1).

192 **2.5 Morphometric analysis**

193 Analysis was carried out on three separate batches of embryos. For each batch, embryos were
194 divided into three groups immediately after injection and each group was allowed to develop
195 until a specific stage: 29 hpf, 4 or 7 dpf respectively. After manual dechorionation of the
196 embryos and larvae (if necessary) with dissection needles, they were deeply anaesthetized in
197 0.02% Tricaine methanesulfonate (MS-222). To facilitate positioning, the embryos or larvae
198 were placed in small Petri dishes containing 3% methylcellulose. Individual pictures were
199 taken using an Axiocam ICc3 camera mounted on a Discovery V.8 stereomicroscope (Zeiss).
200 Morphometric analysis was performed using the software program Axiovision 4.7 (Zeiss) to
201 determine eye surface and body length.

202 **2.6 Immunohistochemical staining**

203 Injected embryos and larvae (manually dechorionated if necessary) of 3 dpf (at 72 hpf), 4 dpf
204 (more precisely at 100 hpf) and 7 dpf were euthanized and subsequently fixed in 4%
205 phosphate-buffered paraformaldehyde overnight at 4°C. The next day they were rinsed with
206 phosphate-buffered saline (PBS) and transferred to a solution of 30% sucrose in PBS. After
207 saturation, the embryos and larvae were embedded in 1.25% agarose/5% sucrose in PBS and
208 again cryoprotected in 30% sucrose in PBS with sodium azide. Cryosections (10 µm) were
209 mounted on glass slides for immunohistochemistry (IHC). The following primary antibodies
210 and dilutions were used: Zpr1 (1:100) and Zpr3 (1:100), both from the Zebrafish International
211 Resource Center (ZIRC, University of Oregon, Eugene, OR, USA), and anti-blue opsin
212 (1:250) and anti-UV opsin (1:500) (Vihtelic et al, 1999). The previously described protocol by
213 Uribe et al. (2007) was used for staining with Zpr1 (labeling both green and red cone
214 photoreceptors) and Zpr3 (labeling rod photoreceptors) (Larison & Bremiller, 1990; Schmitt
215 & Dowling, 1996). The IHC staining for anti-blue and anti-UV opsin, labeling the outer

fragments of blue and UV cones respectively, was performed as follows: the slides were thawed for 20 min at 50°C and permeabilized in PBS/0.1% Triton X-100. Antigen retrieval was carried out in the oven (20 min at 95°C) for anti-UV opsin and in the microwave oven (2 times 5 min at 800W and once at 600W) for anti-blue opsin. After cooling down the sections for 20 min, the endogenous peroxidases were blocked using 0.3% H_2O_2 in methanol for 20 min. After 1 hour of blocking with 2% goat serum and 1% dimethyl sulfoxide in PBS, the primary antibodies (diluted in blocking buffer) were incubated overnight. The following day long amplification was performed. The biotin-conjugated Goat-anti-Rabbit secondary antibody (Dako, 1:300 in PBS/0.05% Triton X-100) was incubated for 45 min after which the complex streptavidin-horseradish peroxidase (Dako, 1:100 in PBS/0.05% Triton X-100) was added for 30 min. Fluorescent labeling was carried out with FITC-tyr (TSA™, Fluorescein System, Perkin Elmer, 1:50 in amplification diluent) for 8 min. Nuclei were counterstained with a 1:1000 dilution of 4',6-diamidino-2-phenylindole (DAPI) in PBS and the sections were mounted with mowiol (Sigma, St. Louis, MO) and glass coverslips. All steps were conducted at room temperature in a humidity chamber with gentle agitation. To minimize any confounding factors during this experiment, we applied three standardizations. We always compared the same (left) eye, and to standardize the position, the section where the optic nerve leaves the retina was taken as a reference point. Finally, the number of rod or cone photoreceptors was expressed per retinal surface (i.e. relative number) since the aforementioned morphometric analysis showed an effect on eye size.

Morphology studies for retinal layer organization were performed on transverse paraffin sections (7 µm) of injected embryos (3 dpf, more precisely 72 hpf) and larvae (7 dpf) after staining with hematoxylin and eosin. All stained sections were imaged with an AxioCam MRc5 camera mounted on a Zeiss Imager.Z1 microscope (Zeiss).

2.7 In situ hybridization

241 In situ hybridization (ISH) was performed on cryosections of uninjected control larvae of
242 72 hpf using digoxigenin-UTP-labeled RNA probes as previously described (Geysens et al,
243 2012; Hidalgo-Sanchez et al, 2005). The hybridization temperature was 67°C for both genes
244 (*dio2* and *dio3b*) and both probes had a length of approximately 800 bp. A sense probe was
245 used as a negative control.

246 **2.8 Optokinetic response test**

247 The optokinetic response (OKR) test was performed as previously described by Neuhauss et
248 al. (1999). In brief, each larva was immobilized in a small Petri dish containing 1%
249 methylcellulose. A circular piece of paper, with an alternating pattern of black and white
250 stripes (1 cm), was manually rotated around the Petri dish (speed: approximately 0.4 cm/s).
251 The reflexive eye movement of the larva was followed under a stereomicroscope. Analysis of
252 the optokinetic response was performed by semi-quantitative scoring starting at 4 dpf up to 7
253 dpf. We divided the response of the larvae into three categories: full, partial and no response.
254 A 'full OKR' corresponds to a larva where the eyes follow the movement of the stripes until
255 they reach the border of the visual field and then return to the original position (i.e. looking
256 straight ahead). During a 'partial OKR' the eyes of the larva get fixed at the border of the
257 visual field and do not perform the returning motion. When reversing the motion of the
258 stripes, they follow the movement again in the opposite direction, until they reach the visual
259 field border at the other site. Larvae with 'no OKR' do not move their eyes at all, which
260 indicates a pronounced default in vision.

261 For each condition (i.e. SCMO, D1D2MO and D3bMO) 10 fish were monitored for reflexive
262 eye movements. This experiment was done on five separate batches, of which two also
263 contained a rescue condition.

264 **2.9 Deiodinase enzyme assays**

For D2 and D3 enzyme activity tests injected larvae (3, 5 and 7 dpf) were sampled, pooled (3 biological replicates of 100 larvae for each condition) and snap frozen on dry ice. *In vitro* deiodination activities were determined in homogenates, freshly prepared from frozen tissues. After homogenizing each sample in 0.6 ml buffer solution (2 mM EDTA, 100 mM phosphate and 1 mM dithiothreitol (DTT), pH 7.2), they were centrifuged at 1500 g for 10 minutes at 4°C. A small fraction of the supernatant was used for the measurement of the protein concentration by the Bradford method using dye reagent concentrate (Bio-Rad, Nazareth, Belgium) (Bradford, 1976). The D2 enzyme assay was performed as previously described in detail (Reyns et al, 2005). D2 activity was measured by incubating homogenate (1.25-1.5 mg protein/ml) with 1 nM T_4, 50.000 cpm [^{125}I]-T_4, 100 nM T_3 (to block D3 interference) and 25 mM DTT for 240 minutes at 37°C. Similar conditions, but containing 100 nM T_4, were used to saturate D2 and determine high Km D1 activity in the homogenates. For the D3 activity test, the conversion of the substrate ^{125}I-T_3 to ^{125}I-T_2 was measured, as previously described (Darras et al, 1996; Darras et al, 1992). The incubation mixture contained homogenate (1.25-1.5 mg protein/ml), 1 nM T_3, 150.000 cpm [^{125}I]-T_3, 1 nM rT_3 (to block D1 interference) and 50 mM DTT and was incubated for 240 min at 37°C. Analysis was done by HPLC, separating ^{125}I-T_3 and ^{125}I-T_2 on a Nucleosil 100-5 C18 column with a mixture of 72% ammonium acetate and 28% acetonitrile. The elution profile was registered by an online radioactivity monitor (LB 506 C-1, Berthold, Vilvoorde, Belgium) and peaks were integrated using the Radiostar program (Berthold).

2.10 Light response

For analysis of the light response SCMO, D1D2MO and D3bMO spontaneously hatched larvae were transferred to individual wells of a 48-well plate. In each plate, larvae from each condition were included and the total sample size for each condition was 48. At 4, 5 and 7 dpf, the swimming behavior of spontaneously hatched larvae was recorded with a Zebrabox

(ViewPoint, Lyon, France) using the video tracking mode with the detection threshold set at 126. Larvae (48 per condition) were tracked individually during 4 min after 30 min dark acclimation. These 4 min consisted of 2 min dark followed by 2 min 100% light (1160.7 lux). First, the average swim speed (mm/s) was calculated for each condition to provide an activity profile (Fig. 8A,C,E). To determine the presence of a significant light response, the swim speed during the 2 min dark preceding the light period was compared to the swim speed during the first 10 s of the light period (Fig. 8B,D,F).

2.11 Statistical analysis

Statistical analysis for cell counting was performed using GraphPad Prism for Windows version 5.00 (GraphPad Software, San Diego CA, USA). If data passed the D'Agostino-Pearson omnibus normality test, they were analyzed by either one-way ANOVA followed by Tukey's post hoc test (for three variables) or by unpaired Student's t test (for two variables). When data did not assume Gaussian distribution, a non-parametric test was performed (Kruskal-Wallis followed by Dunn's post hoc test for three variables and Mann-Whitney for two variables). For the morphometric parameters and relative eye surface, statistical analysis was performed using R for Windows version 3.1.1 and data were analyzed by a mixed effects model. The separate batches were introduced as random effect. For scoring of the OKR, data were analyzed using Chi-square statistics. To determine the presence of a light response, the swim speed during the 2 minutes dark preceding the light period was compared to the swim speed during the first 10 s of the light period using a Wilcoxon-matched pairs signed rank test. A p value below 0.05 was considered statistically significant for all analyses.

3. RESULTS

3.1 Morpholino efficiency

To unravel the function of deiodinases during zebrafish eye development, we used transient KD via injection of MOs blocking either both activating deiodinases (D1+D2) or the main inactivator (D3b). In order to validate these two KD models, we checked the degree and duration of KD efficiency by deiodinase activity tests at 3 and 7 dpf. These data showed that at 3 dpf both MO treatments reduced enzyme activity to less than 10% at the physiologically most relevant low Km substrate concentration (Table 2). Their efficiency was markedly reduced but not completely abolished at 7 dpf. Noticeably, the efficiency of the D1+D2 morpholino and the D3b morpholino seemed to disappear at a similar rate since deiodination percentages of both MO treatments at 7 dpf were almost comparable.

3.2 Transcriptome analysis

Previous transcriptome analysis of the head identified the phototransduction pathway as one of the most important gene ontology classes affected in deiodinase KD zebrafish (Bagci et al, 2015), including visual perception and the G-protein coupled receptor signaling pathway. In the present study, an in-depth pathway analysis revealed an influence on almost all components of the excitation and the recovery pathway, as well as on retinoid recycling. Although both KD conditions affected gene expression in the same direction, D3bMO clearly had the most pronounced effect: more genes were affected in D3bMO larvae and also the level of downregulation was stronger (supplementary Fig.S1). For the excitation pathway, genes from the following components were downregulated in both KD conditions: receptors (*opn1sw1*, *opn1sw2*, *opn1mw1*, *opn1mw2*, *opn1lw2*, *rho*), G proteins (*gnat1*, *gnat2*, *gnb5b*, *gnb3b*, *gngt1*, *gngt2a*, *gngt2b*), phosducin (*pdcb*), phosphodiesterases (*pde6c*, *pde6h*, zgc:73359), guanylate cyclase (*gc3*, *guca1c*) and GTP metabolism (*guk1*). The transcripts only affected after KD of D3b were: receptor (*rgra*), G protein (*gnao1b*), phosphodiesterase (*pde6a*), sodium/calcium channel (LOC572249) and GTP metabolism (*pnp6*). Also transcripts that belong to the recovery pathway were downregulated in D1D2MO larvae as well as

D3bMO larvae: regulator of G protein signaling (*rgs9*), receptor kinase (*grk1b*), recoverin (*rcv1*) and arrestin (*sagb*, *arr3a*, *arr3b*). Additional transcripts in the D3bMO condition were: regulator of G protein (*rgs11*, *rgs8*) and arrestin (*saga*). Finally, also several components of retinoid recycling were affected: LOC556575, *rlbp1a*, *rlbp1b* and *irbp* in both KD conditions and *rpe65a* and *rbp4l* specifically for D3bMO larvae. A detailed scheme showing the links between the different processes and genes is represented in Fig. 1 that includes every molecular component that was affected after deiodinase KD.

Not only the phototransduction and retinoid recycling pathways were severely disturbed in D3bMO larvae, also other components of the eye and its function were affected. The heatmaps in Fig. 2B show that several mRNAs related to retinal, corneal and lens structure were downregulated. Also the metabolism of the three retinal neurotransmitters (glutamate, glycine and gamma-aminobutyric acid (GABA)) was markedly altered (Fig. 2A). On the contrary, practically no structural or neurotransmitter related genes were influenced in D1D2MO larvae. The degree of downregulation for the few genes that were affected was also less severe (Fig. 2).

From these microarray data, we hypothesized that levels of transcripts involved in phototransduction and visual cycle were decreased specifically in the eyes of both deiodinase KD groups. In order to validate this hypothesis, 10 transcripts involved in phototransduction and visual cycle, that were significantly differentially expressed in the microarray analysis of heads of deiodinase KD fish (Fig. 1 and supplementary Fig. S1), were selected for validation by Q-PCR in the eyes of both deiodinase KD conditions. The candidate genes were chosen in such way that both the excitation and the recovery pathway were represented: *opn1sw1*, *opn1sw2*, *opn1mw1*, *opn1lw2*, *rho*, *pde6a*, *pde6h*, *grk1b*, *arr3a* and *rpe65a*. All 10 genes tested were strongly downregulated compared to the SCMO group (Table 3), which clearly corroborates the microarray data. In line with an eye-specific effect, the relative

downregulation in the Q-PCR analysis was in general stronger compared to the microarray results obtained from whole head samples.

3.3 Localization of D2 and D3b in the zebrafish retina

Two research groups have already shown that *dio2* and *dio3b* are both expressed in the retina during early stages (Guo et al, 2014; Thisse et al, 2003), but these experiments were performed on whole-mount embryos and larvae. To investigate retinal expression in more detail we carried out ISH on cryosections of the eye of 3 dpf uninjected control larvae. Fig. 3A shows intense staining for *dio2* throughout all layers of the retina, except for the inner plexiform layer and with the highest signal in the outer plexiform and outer nuclear layer. Although the overall signal with the *dio3* probe is less intense, we found that the inactivating deiodinase is also expressed in all retinal layers except the inner plexiform layer (Fig. 3B). The highest signal is present in the outer plexiform and inner nuclear layer, but staining is also present in the outer nuclear and ganglion cell layer.

3.4 Effects on eye size and retinal layer organization.

To analyze the effect of deiodinase KD on zebrafish eye morphology, we first measured eye size at 29 hpf, 4 and 7 dpf. Figure 4A shows the combined eye size measurements of three batches. At 29 hpf morphants of both KD groups had a significantly smaller eye compared to SCMO embryos. While D1D2MO larvae already caught up with the control group by 4 dpf, the defect persisted for D3bMO larvae, even at 7 dpf. We also observed that both KD conditions had a significant reduction in body length at 29 hpf and 4 dpf but they caught up by 7 dpf (Fig. 4B). To assess whether the decreased eye size of the KD fish was a specific effect or an indirect consequence of delayed growth, we followed an approach similar to what has been described for weight-length relationships (condition factor) in fish (Jones et al, 1999; Le Cren, 1951; Richter et al, 2000). We only used the data obtained at 4 and 7 dpf since the

eye of zebrafish embryos does not grow linearly proportional to the body length during the first 2 dpf, but follows an exponential pattern (supplementary Fig. S2A) and 29 hpf data can therefore not be included in the same equation. Supplementary Fig. S2B shows a representative growth curve for control fish from 3 to 7 dpf, showing a linear correlation between eye size and body length. For each individual fish in every condition, a factor that we denote as Relative Eye Surface (RES) was then calculated by dividing the 'observed eye surface' by the 'expected eye surface' based on the length of the larva. For each batch RES was calculated based on the linear regression model for control animals of that specific batch. Fig. 4C shows the RES values from the three batches combined and these data were statistically analyzed by a mixed effects model (with batch as random effect) with the software package R. The D1D2MO larvae had a significantly higher RES than SCMO larvae at 4 dpf while the RES for D3bMO larvae was significantly reduced at both stages indicative of a more persistent effect on eye size.

To investigate whether a smaller eye size was also accompanied by an aberrant retinal morphology, we prepared transverse paraffin sections of the head. At 3 dpf D1D2MO larvae (Fig. 5B) showed an overall normal eye morphology and retinal layer organization but the ganglion cell layer (GCL) was wider and less dense compared to SCMO (Fig. 5A). In D3bMO larvae however, there was a marked disorganization across all layers of the retina (Fig. 5C). By 7 dpf, the layer organization of both morphants resembled the normal morphology of SCMO, although small variations in the thickness and density of the GCL and inner nuclear layer persisted in the D3bMO group (Fig. 5D-F).

3.5 Effects on the number of rod and cone photoreceptors.

Since the transcriptome analysis revealed a clear downregulation of opsins from all photoreceptors, we decided to investigate whether this was accompanied by a reduction in the

number of cones and rods. In a first experiment we performed an IHC staining with the Zpr1 and Zpr3 antibodies. Zpr1 binds to the protein encoded by *arr3a* that forms a key molecule in the photoresponse recovery pathway and is expressed in green and red cone photoreceptors (which always occur as a pair), while Zpr3 binds to rhodopsin, the opsin present in rods. At 3 dpf, both KD conditions showed a significant reduction in the relative number of green and red cones (expressed per retinal surface area). By 4 dpf, D1D2 morphants had already caught up with the control group while D3b morphants did not (data not shown). The relative rod number was also decreased in both KD conditions at 3 dpf, although not significantly for D1D2MO (Fig. 6M). The next day, also D3bMO larvae caught up with the control group for relative rod number (Table 4).

In a second experiment, we studied the effects on cones in more detail, using two additional antisera binding to the opsins in the outer segment of UV and blue cones respectively and also including 7 dpf to determine the persistency of reduction for the 4 cone types. These data showed that in both KD conditions all 4 cone types were significantly reduced compared to the SCMO group at 3 dpf (Fig. 6N-P), thereby also confirming the results of the previous experiment regarding the green and red cones. This difference was still present at 4 dpf for all cone types, but only in the D3bMO group (Table 4). By 7 dpf, relative cone numbers in D3bMO larvae were no longer reduced (Table 4). Representative pictures of the 3 dpf larvae are shown in Fig. 6A-L.

3.6 Effects on eye optokinetic response.

We finally addressed the question whether the KD larvae also had defects at the functional level. Therefore, we first performed an optokinetic response (OKR) test. The OKR is described to start around 95 hpf (Neuhauss et al, 1999), and we tested the response at 100 hpf which corresponds exactly to the stage used for the IHC stainings. Results of the first three

batches (data not shown) indicated that all larvae of the SCMO as well as the D1D2MO condition possessed a full OKR at 100 hpf, suggesting that these larvae had functional sight and responded normally to the stimulus. However, only about 30% of the D3bMO larvae possessed a normal OKR at this stage. The majority did not move their eyes at all or displayed only a partial response. To investigate whether or not the vision of these larvae improved over time, we followed them until 7 dpf. At this stage still a significant part (40%) of the D3bMO larvae showed no OKR at all.

To demonstrate the specificity of the observed effect, we repeated the OKR test on two additional batches (Fig. 7), including a rescue condition for the D3bMO using human *DIO3* mRNA that is not targeted by the zebrafish D3b morpholino. The D1D2MO, D3bMO and SCMO condition displayed the same pattern of responses as before. In addition, approximately 50% of the larvae of the rescue condition already possessed a full OKR at 100 hpf (Fig. 7A) and all of them displayed a normal OKR by 7 dpf (Fig. 7B).

3.7 Effects on light response.

Based on the transcriptome data we also hypothesized that deiodinase deficient larvae might be less sensitive to a light stimulus. This assumption was tested in a behavioral study by analyzing the response during 10 seconds of light after 2 minutes in the dark (preceded by 30 min of dark acclimation). A normal zebrafish larva responds to this light stimulus by a peak in activity (measured as travelled distance per second). At 4 dpf, only SCMO displayed a significant light response (Fig. 8B). The next day, D1D2MO as well as SCMO had a clear response as indicated by a significant increase of activity during the light stimulus while D3bMO still showed no response (Fig. 8D). By 7 dpf however, all larvae exhibited a normal light response (Fig. 8F). Average activity patterns throughout the test period are shown in the left column of Fig. 8.

4. DISCUSSION

The present study clearly shows that KD of both activating and inactivating deiodinases profoundly disturbs zebrafish eye development starting from the gene expression level. It is known that eye development in zebrafish is a process very susceptible to disturbances, not merely related to THs. The loss of photoreceptors is a common phenotypical property of several mutant zebrafish lines and often correlates with defects in the OKR (Brockerhoff, 2006; Brockerhoff et al, 2003; Huang & Neuhauss, 2008; Neuhauss et al, 1999). We showed that TH imbalance caused by D3b deficiency results in a similar phenotype. These characteristics were not due to non-specific effects of the MO since the functional defect in OKR could be rescued by injection of human *DIO3* mRNA. Also in our D1+D2 deficiency model we found a reduction in the number of photoreceptors, but less severe and persistent compared to D3bMO.

There are several reports demonstrating the influence of hypothyroidism (lowered circulating TH levels) on eye development (Li et al, 2012; Navegantes et al, 1996; Pinazo-Duran et al, 2005; Reider & Connaughton, 2014; Sevilla-Romero et al, 2002). The function of the different deiodinases however, is not well understood. The only available deiodinase deficient model where defects at the level of the eye have been observed, is the D3 knockout mouse (Ng et al, 2010). Adult D3-null mice lack approximately 80% of both M (median wavelength, green) and S (short wavelength, blue) cone photoreceptors, as a result of neonatal cell death, while the rods remain intact. We confirmed that in zebrafish too D3 deficiency has a clear detrimental effect on cone development. In addition we found in our model that rods were also affected although to a lesser extent.

4.1 Deiodinase KD reduces the number of rod and cone photoreceptors

We were the first to investigate the effect of deiodinase KD on gene expression in the head region of zebrafish embryos using microarray analysis and found that eye development and phototransduction were the major pathways that were affected. Quantitative PCR on eye samples confirmed downregulation of several genes involved in the excitation as well as the recovery pathway of phototransduction. Another research group published results from a transcriptome analysis in zebrafish embryos after administration of exogenous T_3 and also saw clear changes in the expression of retina-related genes (Pelayo et al, 2012), suggesting that in our D3-deficient fish the changes in gene expression may be due to increased T_3 signaling.

Based on the present data combined with the information from the extensive transcriptome analysis described in our previous report (Bagci et al, 2015), we can propose molecular mechanisms resulting in the loss of rods and cones (Fig. 6). Several transcripts that are part of the induction and regulation of apoptotic processes (for example *tp53*, *phlda3*, *chac1*, *dusp2*) are differentially transcribed in the D3bMO condition (Bagci et al, 2015). In addition, other processes are affected in our D3 deficiency model. For instance the gene *odc1*, upregulated in D3bMO larvae, is essential for photoreceptor development since disruption of this gene induces defects in the outer segments (Gross et al, 2005). It is possible that inappropriate timing/level of gene expression disrupts photoreceptor development. Photoreceptor differentiation seems to be affected as well. *Crb2b*, the crumbs gene which is not expressed during early eye development is normally upregulated by 72 hpf in differentiating photoreceptors cells (Omori & Malicki, 2006), but is in fact strongly downregulated in D3bMO fish. A similar trend applies to *apc*. This gene is crucial for photoreceptor cell differentiation, but is downregulated in D3bMO larvae. Additionally, *apc* operates via Wnt signaling, a pathway involved in photoreceptor differentiation (Nadauld et al, 2006). Other components of the Wnt signaling pathway, such as r*spo1* and *sybu*, are also differentially

transcribed in D3bMO larvae. There is evidence in literature that the ligand retinoic acid is important during zebrafish photoreceptor differentiation because of its dynamic equilibrium with THs (Suliman & Novales Flamarique, 2014). In this study we found proof of this relationship as well. The already mentioned *apc* gene is known to be involved in retinoic acid biosynthesis, so its downregulation probably results in a decrease in retinoic acid availability. Furthermore, the transcriptome data may indicate a possible compensatory mechanism, since the genes *crabp1b* and *crabp2a*, important mediators of retinoic acid action (Giguere, 1994), are both upregulated in D3b morphants. Crabp proteins transport retinoic acid intracellularly so that it can bind to its nuclear receptors (such as TRs) and exert its function via influence on gene transcription (Cai et al, 2012; Napoli, 1993).

It is known that TRs form an essential link in the molecular mechanisms underlying photoreceptor development in mice and regulate the relative abundancy of different cone types (Ng et al, 2001). In zebrafish embryos there is evidence for a similar role of TRβ2 in cone development. KD of this receptor did not change total cone density but severely reduced the number of L (long wavelength, red) cones while increasing the number of UV cones (Suzuki et al, 2013). The effects observed in our D3b KD model were more pronounced showing a reduction in all four cone populations at early stages, thereby also reducing total cone density. The results for D3bMO zebrafish are in line with those found in D3-null mice that also show a severe reduction in total cone number (Ng et al, 2010). Interestingly, the eye phenotype of D3-null mice was partially rescued following combined knockout of TRβ2, but only restoring the cones responsive to short wavelengths (Ng et al, 2010). It would be interesting to find out if combined KD of TRβ and D3b in zebrafish would lead to a similar cone type-specific rescue.

Taken together the above information clearly indicates that premature exposure to excessive TH signaling is detrimental for correct cone differentiation. However, we also observed a negative effect of D1+D2-KD on photoreceptor number (Fig. 6, Table 4). Interestingly, the underlying mechanisms may differ from the ones described above for D3bMO since the above mentioned transcripts related to Wnt signaling and apoptosis were not differentially expressed in D1D2MO. To our knowledge, no results have been published on D1 or D2 knockout mice in relation to eye or photoreceptor development. The fact that we do observe an apparent phenotype in our D1+D2 deficient model may be due to the fact that zebrafish express both D2 and D3 in all layers of the developing retina (Fig. 3), while in mice predominantly D3 is expressed in the prenatal retina (Ng et al, 2010). It may seem surprising that blocking of the TH-activating pathway results in a similar, although less pronounced, phenotype as silencing of the TH-inactivating pathway, but it is certainly not uncommon for excessive and depleted amounts of THs to cause parallel developmental defects (Elsalini & Rohr, 2003; Liu & Chan, 2002; Reddy & Lam, 1991). There seems to be a given threshold for accurate TR signaling and TH concentrations above or below this threshold will have detrimental effects.

Eye surface is decreased after deiodinase KD and retinal lamination is mildly altered

We found that knocking down the TH-activating or the TH-inactivating pathway (and hence the resulting hypothyroidism/hyperthyroidism) both diminished eye surface in the first days of development (Fig. 4). Several reports have been published demonstrating a link between hypothyroidism and a reduction in eye size, in fish as well as other vertebrates (Gamborino et al, 2001; Li et al, 2012; Navegantes et al, 1996; Pinazo-Duran et al, 2005; Reider & Connaughton, 2014; Sevilla-Romero et al, 2002). To our knowledge, only one paper reported on hyperthyroidism, showing that zebrafish embryos have a reduced eye size after T_3

554 supplementation (Pelayo et al, 2012). Our study showed a significant reduction in absolute
555 eye size at 29 hpf in both KD conditions. However, calculating the relative eye surface (RES)
556 at later stages revealed a divergent pattern. D1D2MO larvae caught up with the control fish
557 by 4 dpf and even had a transiently increased RES, suggesting that the delay in eye growth
558 caught up more rapidly than the delay in total body growth. In contrast, the RES for D3bMO
559 larvae was still significantly reduced at 7 dpf, suggesting that the reduction in eye size does
560 not simply reflect a general delay in development, but represents a noticeable defect that
561 persists at later stages.

562 This reduction in eye size was also accompanied by an aberrant retinal layer organization
563 (Fig. 5). It has been reported that hypothyroid zebrafish embryos (treated with MMI until 70
564 hpf) display a transient enlargement of the GCL (Reider & Connaughton, 2014) which would
565 correspond to the transient effect observed in our D1D2MO condition. D3b morphants
566 however showed a severe and long-term disorganization of the retinal layers. A potential
567 mechanism can be found in our earlier transcriptome study (Bagci et al, 2015), revealing a
568 strong downregulation of the *rs1* transcript in D3bMO fish (and specifically not in D1D2MO
569 fish) at 3 dpf. *Rs1* transcription in zebrafish retina is normally detectable from 42 hpf and is
570 involved in cell-cell interaction in the layers of the retina (Thisse & Thisse, 2004; Yokoi et al,
571 2009). Mutations in the human orthologue cause the eye disease retinoschisis which is
572 characterized by the abnormal splitting of the neurosensory layers of the retina (Tantri et al,
573 2004).

574 **4.2 D3bMO larvae possess visual impairments**

575 Using the optokinetic response test, a reliable test for detecting visual impairments in
576 zebrafish larvae (Brockerhoff, 2006; Neuhauss et al, 1999), we found that a vast majority of
577 D3bMO larvae showed an abnormal response at 100 hpf and even at 7 dpf (Fig. 7). The loss

of photoreceptors in the D3bMO group could be an essential element causing the OKR defects. For example, zebrafish *odc1* mutants (with photoreceptor defects, see above) also show only a weak OKR (Gross et al, 2005). Interestingly, part of the D3b morphants showed a partial OKR even at 7 dpf. In our experiments, this involved the execution of the first part of the response (i.e. smooth movement of the eyes in the direction of the rotation), but without a fast reset after reaching the border of the visual field. This may point to defects at the level of the eye muscles, since several transcripts related to muscle development and contraction (for example *myhz1.1*, *myhz1.2*, *tnni2a.4*) were only affected by D3bMO, and not by D1D2MO (Bagci et al, 2015) and D1D2 morphants all showed a normal OKR at 100 hpf.

More profound analysis of larval vision was performed using the light response test revealing that, in contrast to control fish and D1D2 morphants, D3b morphants do not yet react to the switch from dark to light at 5 dpf (Fig. 8D). These results are in agreement with our finding that the phototransduction pathways are affected in every single step of the way. Genes specifically related to photoreceptor activity, for example the cone opsins (*opn1sw1*, *opn1sw2*, *opn1mw1*, *opn1mw2*, *opn1lw2*), the rod opsin (*rho*) and *grk7a*, are more strongly downregulated in the D3bMO condition compared to the D1D2MO condition (Supplementary Fig. S1). At this point, we cannot exclude the implication of an impaired swimming capacity. In two previous studies we indeed showed that swimming activity of D3bMO was reduced together with downregulation of transcripts related to muscle in abdomen and tail of 72 hpf-old zebrafish larvae (Bagci et al, 2015; Heijlen et al, 2014). Both mechanisms could therefore contribute to the observed reduced activity pattern as a response to a light stimulus. When the larvae reached the age of 7 dpf, the difference between the D3bMO and the control group in the light response test had also disappeared (Fig. 8F) although at this stage D3bMO larvae still showed defects in the OKR test (Fig. 7) and they still have a reduced mobility (unpublished results). While this may seem surprising, the milder phenotype in the light

603 response test compared to the OKR test could partially be due to the experimental setup. In
604 the light response test, only spontaneously hatched larvae were included and followed until 7
605 dpf while this was not the case for the other tests where animals were manually dechorionated
606 if necessary. Since previous results from our research group showed that KD of D3b severely
607 delays the time of hatching (Heijlen et al, 2014) this approach probably excluded to the ones
608 that were most severely affected by the KD.

609 ## 5. CONCLUSION

610 To summarize, silencing of the activating as well as the inactivating deiodination pathway
611 disturbs zebrafish eye development at the level of gene expression, morphology and function,
612 but a premature exposure to high T_3 levels, i.e. the D3b-KD model, results in more severe and
613 persistent defects. The D1D2MO phenotype seems to reflect primarily a general delay in early
614 development, while D3bMO leads to more persistent defects, as shown by an aberrant RES,
615 retinal lamination and OKR at 7 dpf. It should be noted that although we can efficiently block
616 the TH activating or inactivating pathway by MO injection, this technique only provokes a
617 transient KD that is already strongly reduced by 7 dpf. As such the defects in eye
618 development and function may be more persistent for both conditions when deiodinase
619 expression is blocked permanently, a question that can be answered once stable mutant
620 zebrafish lines with loss-of-function for deiodinases become available.

621 ## 6. ACKNOWLEDGEMENTS

622 The authors kindly thank Lut Noterdaeme and Lieve Geenen for their technical assistance and
623 Véronique Brouwers and Evelien Herinckx for help in maintaining the zebrafish facility. We
624 also thank Prof. T. Visser (Erasmus University Medical Center, Rotterdam) for providing the
625 human *DIO3* cDNA, Dr. Wouter Dehaes (Section Animal Physiology and Neurobiology, KU
626 Leuven) for help with statistical analysis in R and Pieter Vancamp (Research group

627 Comparative Endocrinology, KU Leuven) for performing the ISH experiments. This work
628 was supported by a research grant from the ‘Fonds Wetenschappelijk Onderzoek –
629 Vlaanderen’ (FWO G.0528.10) and by a travel grant from the ‘Academische Stichting
630 Leuven’.

631

7. REFERENCES

Allison WT, Dann SG, Veldhoen KM, Hawryshyn CW (2006) Degeneration and regeneration of ultraviolet cone photoreceptors during development in rainbow trout. *The Journal of comparative neurology* **499:** 702-715

Bagci E, Heijlen M, Vergauwen L, Hagenaars A, Houbrechts AM, Esguerra CV, Blust R, Darras VM, Knapen D (2015) Deiodinase Knockdown during Early Zebrafish Development Affects Growth, Development, Energy Metabolism, Motility and Phototransduction. *PloS one* **10:** e0123285

Bianco AC, Kim BW (2006) Deiodinases: implications of the local control of thyroid hormone action. *The Journal of clinical investigation* **116:** 2571-2579

Bibliowicz J, Gross JM (2009) Expanded progenitor populations, vitreo-retinal abnormalities, and Muller glial reactivity in the zebrafish leprechaun/patched2 retina. *BMC developmental biology* **9:** 52

Bradford MM (1976) A rapid and sensitive method for the quantitation of microgram quantities of protein utilizing the principle of protein-dye binding. *Analytical biochemistry* **72:** 248-254

Brockerhoff SE (2006) Measuring the optokinetic response of zebrafish larvae. *Nature protocols* **1:** 2448-2451

Brockerhoff SE, Rieke F, Matthews HR, Taylor MR, Kennedy B, Ankoudinova I, Niemi GA, Tucker CL, Xiao M, Cilluffo MC, Fain GL, Hurley JB (2003) Light stimulates a transducin-independent increase of cytoplasmic Ca2+ and suppression of current in cones from the zebrafish mutant nof. *The Journal of neuroscience : the official journal of the Society for Neuroscience* **23:** 470-480

Cai AQ, Radtke K, Linville A, Lander AD, Nie Q, Schilling TF (2012) Cellular retinoic acid-binding proteins are essential for hindbrain patterning and signal robustness in zebrafish. *Development* **139:** 2150-2155

CSH Protocols (2011) Recipe Danieau's solution (30x). *Cold Spring Harbor Laboratory Press***:** doi:10.1101/pdb.rec12467

Dahm R, Geisler R (2006) Learning from small fry: the zebrafish as a genetic model organism for aquaculture fish species. *Mar Biotechnol (NY)* **8:** 329-345

Darras VM, Kotanen SP, Geris KL, Berghman LR, Kuhn ER (1996) Plasma thyroid hormone levels and iodothyronine deiodinase activity following an acute glucocorticoid challenge in embryonic compared with posthatch chickens. *General and comparative endocrinology* **104:** 203-212

677 Darras VM, Visser TJ, Berghman LR, Kuhn ER (1992) Ontogeny of type I and type III
678 deiodinase activities in embryonic and posthatch chicks: relationship with changes in
679 plasma triiodothyronine and growth hormone levels. *Comparative biochemistry and*
680 *physiology Comparative physiology* **103:** 131-136

681
682 Dowling JE (1987) *The Retina: An Approachable Part of the Brain*, Cambridge, MA.: The
683 Belknap Press of Harvard University Press.

684
685 Ebrey T, Koutalos Y (2001) Vertebrate photoreceptors. *Progress in retinal and eye*
686 *research* **20:** 49-94

687
688 Elsalini OA, Rohr KB (2003) Phenylthiourea disrupts thyroid function in developing
689 zebrafish. *Development Genes and Evolution* **212:** 593-598

690
691 Fischer AJ, Bongini R, Bastaki N, Sherwood P (2011) The maturation of photoreceptors in
692 the avian retina is stimulated by thyroid hormone. *Neuroscience* **178:** 250-260

693
694 Gamborino MJ, Sevilla-Romero E, Munoz A, Hernandez-Yago J, Renau-Piqueras J, Pinazo-
695 Duran MD (2001) Role of thyroid hormone in craniofacial and eye development using a
696 rat model. *Ophthalmic Res* **33:** 283-291

697
698 Germain DL, Galton VA, Hernandez A (2009) Defining the roles of the iodothyronine
699 deiodinases: current concepts and challenges. *Endocrinology* **150:** 1097-1107

700
701 Geysens S, Ferran JL, Van Herck SL, Tylzanowski P, Puelles L, Darras VM (2012)
702 Dynamic mRNA distribution pattern of thyroid hormone transporters and deiodinases
703 during early embryonic chicken brain development. *Neuroscience* **221:** 69-85

704
705 Giguere V (1994) Retinoic acid receptors and cellular retinoid binding proteins: complex
706 interplay in retinoid signaling. *Endocrine reviews* **15:** 61-79

707
708 Gonzalez P, Baudrimont M, Boudou A, Bourdineaud JP (2006) Comparative effects of
709 direct cadmium contamination on gene expression in gills, liver, skeletal muscles and
710 brain of the zebrafish (Danio rerio). *Biometals : an international journal on the role of*
711 *metal ions in biology, biochemistry, and medicine* **19:** 225-235

712
713 Gross JM, Perkins BD, Amsterdam A, Egana A, Darland T, Matsui JI, Sciascia S, Hopkins
714 N, Dowling JE (2005) Identification of zebrafish insertional mutants with defects in visual
715 system development and function. *Genetics* **170:** 245-261

716
717 Guo C, Chen X, Song H, Maynard MA, Zhou Y, Lobanov AV, Gladyshev VN, Ganis JJ,
718 Wiley D, Jugo RH, Lee NY, Castroneves LA, Zon LI, Scanlan TS, Feldman HA, Huang SA
719 (2014) Intrinsic Expression of a Multiexon Type 3 Deiodinase Gene Controls Zebrafish
720 Embryo Size. *Endocrinology***:** en20132029

721

Havis E, Le Mevel S, Morvan Dubois G, Shi DL, Scanlan TS, Demeneix BA, Sachs LM (2006) Unliganded thyroid hormone receptor is essential for Xenopus laevis eye development. *The EMBO journal* **25:** 4943-4951

Heijlen M, Houbrechts AM, Bagci E, Van Herck SL, Kersseboom S, Esguerra CV, Blust R, Visser TJ, Knapen D, Darras VM (2014) Knockdown of type 3 iodothyronine deiodinase severely perturbs both embryonic and early larval development in zebrafish. *Endocrinology* **155:** 1547-1559

Hidalgo-Sanchez M, Martinez-de-la-Torre M, Alvarado-Mallart RM, Puelles L (2005) A distinct preisthmic histogenetic domain is defined by overlap of Otx2 and Pax2 gene expression in the avian caudal midbrain. *The Journal of comparative neurology* **483:** 17-29

Higdon CW, Mitra RD, Johnson SL (2013) Gene expression analysis of zebrafish melanocytes, iridophores, and retinal pigmented epithelium reveals indicators of biological function and developmental origin. *PloS one* **8:** e67801

Huang YY, Neuhauss SC (2008) The optokinetic response in zebrafish and its applications. *Frontiers in bioscience : a journal and virtual library* **13:** 1899-1916

Jones RE, Petrell RJ, Pauly D (1999) Using modified length–weight relationships to assess the condition of fish. *Aquacultural Engineering* **20:** 261-276

Kelley MW, Turner JK, Reh TA (1995) Ligands of steroid/thyroid receptors induce cone photoreceptors in vertebrate retina. *Development* **121:** 3777-3785

Krishnan K, Salomonis N, Guo S (2008) Identification of Spt5 target genes in zebrafish development reveals its dual activity in vivo. *PloS one* **3:** e3621

Laranjeiro R, Whitmore D (2014) Transcription factors involved in retinogenesis are co-opted by the circadian clock following photoreceptor differentiation. *Development* **141:** 2644-2656

Larison KD, Bremiller R (1990) Early onset of phenotype and cell patterning in the embryonic zebrafish retina. *Development* **109:** 567-576

Le Cren ED (1951) The length-weight relationship and seasonal cycle in gonad weight and condition in the perch (Perca Flucaitilis). *Journal of Animal Ecology* **20:** 201-2019

Li Z, Ptak D, Zhang L, Walls EK, Zhong W, Leung YF (2012) Phenylthiourea specifically reduces zebrafish eye size. *PloS one* **7:** e40132

Liu F, Chen J, Yu S, Raghupathy RK, Liu X, Qin Y, Li C, Huang M, Liao S, Wang J, Zou J, Shu X, Tang Z, Liu M (2015) Knockout of RP2 decreases GRK1 and rod transducin subunits and leads to photoreceptor degeneration in zebrafish. *Human molecular genetics* **24:** 4648-4659

Liu YW, Chan WK (2002) Thyroid hormones are important for embryonic to larval transitory phase in zebrafish. *Differentiation; research in biological diversity* **70:** 36-45

Ma H, Thapa A, Morris L, Redmond TM, Baehr W, Ding XQ (2014) Suppressing thyroid hormone signaling preserves cone photoreceptors in mouse models of retinal degeneration. *Proceedings of the National Academy of Sciences of the United States of America* **111:** 3602-3607

Mader MM, Cameron DA (2004) Photoreceptor differentiation during retinal development, growth, and regeneration in a metamorphic vertebrate. *The Journal of neuroscience : the official journal of the Society for Neuroscience* **24:** 11463-11472

Mader MM, Cameron DA (2006) Effects of induced systemic hypothyroidism upon the retina: regulation of thyroid hormone receptor alpha and photoreceptor production. *Molecular vision* **12:** 915-930

Malicki J, Neuhauss SC, Schier AF, Solnica-Krezel L, Stemple DL, Stainier DY, Abdelilah S, Zwartkruis F, Rangini Z, Driever W (1996) Mutations affecting development of the zebrafish retina. *Development* **123:** 263-273

Marsh-Armstrong N, Huang H, Remo BF, Liu TT, Brown DD (1999) Asymmetric growth and development of the Xenopus laevis retina during metamorphosis is controlled by type III deiodinase. *Neuron* **24:** 871-878

Nadauld LD, Chidester S, Shelton DN, Rai K, Broadbent T, Sandoval IT, Peterson PW, Manos EJ, Ireland CM, Yost HJ, Jones DA (2006) Dual roles for adenomatous polyposis coli in regulating retinoic acid biosynthesis and Wnt during ocular development. *Proceedings of the National Academy of Sciences of the United States of America* **103:** 13409-13414

Napoli JL (1993) Biosynthesis and metabolism of retinoic acid: roles of CRBP and CRABP in retinoic acid: roles of CRBP and CRABP in retinoic acid homeostasis. *The Journal of nutrition* **123:** 362-366

Navegantes LC, Silveira LC, Santos GL (1996) Effect of congenital hypothyroidism on cell density in the ganglion cell layer of the rat retina. *Brazilian journal of medical and biological research = Revista brasileira de pesquisas medicas e biologicas / Sociedade Brasileira de Biofisica [et al]* **29:** 665-668

Neuhauss SC, Biehlmaier O, Seeliger MW, Das T, Kohler K, Harris WA, Baier H (1999) Genetic disorders of vision revealed by a behavioral screen of 400 essential loci in zebrafish. *The Journal of neuroscience : the official journal of the Society for Neuroscience* **19:** 8603-8615

Ng L, Hurley JB, Dierks B, Srinivas M, Salto C, Vennstrom B, Reh TA, Forrest D (2001) A thyroid hormone receptor that is required for the development of green cone photoreceptors. *Nature genetics* **27:** 94-98

Ng L, Lyubarsky A, Nikonov SS, Ma M, Srinivas M, Kefas B, St Germain DL, Hernandez A, Pugh EN, Jr., Forrest D (2010) Type 3 deiodinase, a thyroid-hormone-inactivating enzyme, controls survival and maturation of cone photoreceptors. *The Journal of neuroscience : the official journal of the Society for Neuroscience* **30:** 3347-3357

Omori Y, Malicki J (2006) oko meduzy and related crumbs genes are determinants of apical cell features in the vertebrate embryo. *Current biology : CB* **16:** 945-957

Pelayo S, Oliveira E, Thienpont B, Babin PJ, Raldua D, Andre M, Pina B (2012) Triiodothyronine-induced changes in the zebrafish transcriptome during the eleutheroembryonic stage: implications for bisphenol A developmental toxicity. *Aquat Toxicol* **110-111:** 114-122

Pinazo-Duran MD, Iborra FJ, Pons S, Sevilla-Romero E, Gallego-Pinazo R, Munoz A (2005) Postnatal thyroid hormone supplementation rescues developmental abnormalities induced by congenital-neonatal hypothyroidism in the rat retina. *Ophthalmic Res* **37:** 225-234

Reddy PK, Lam TJ (1991) Effect of thyroid hormones on hatching in the tilapia, Oreochromis mossambicus. *General and comparative endocrinology* **81:** 484-491

Reider M, Connaughton VP (2014) Effects of low-dose embryonic thyroid disruption and rearing temperature on the development of the eye and retina in zebrafish. *Birth defects research Part B, Developmental and reproductive toxicology* **101:** 347-354

Rey S, Boltana S, Vargas R, Roher N, Mackenzie S (2013) Combining animal personalities with transcriptomics resolves individual variation within a wild-type zebrafish population and identifies underpinning molecular differences in brain function. *Molecular ecology* **22:** 6100-6115

Reyns GE, Verhoelst CH, Kuhn ER, Darras VM, Van der Geyten S (2005) Regulation of thyroid hormone availability in liver and brain by glucocorticoids. *General and comparative endocrinology* **140:** 101-108

Richter H, Luckstadt C, Focken UL, K. B (2000) An improved procedure to assess fish condition on the basis of length-weight relationships. *Archive of Fishery and Marine Research* **48:** 226-235

Roberts MR, Srinivas M, Forrest D, Morreale de Escobar G, Reh TA (2006) Making the gradient: thyroid hormone regulates cone opsin expression in the developing mouse retina. *Proceedings of the National Academy of Sciences of the United States of America* **103:** 6218-6223

Schmitt EA, Dowling JE (1996) Comparison of topographical patterns of ganglion and photoreceptor cell differentiation in the retina of the zebrafish, Danio rerio. *The Journal of comparative neurology* **371:** 222-234

865 Sevilla-Romero E, Munoz A, Pinazo-Duran MD (2002) Low thyroid hormone levels impair
866 the perinatal development of the rat retina. *Ophthalmic Res* **34:** 181-191

867
868 Smyth GK (2004) Linear models and empirical bayes methods for assessing differential
869 expression in microarray experiments. *Statistical applications in genetics and molecular*
870 *biology* **3:** Article3

871
872 Suliman T, Novales Flamarique I (2014) Visual pigments and opsin expression in the
873 juveniles of three species of fish (rainbow trout, zebrafish, and killifish) following
874 prolonged exposure to thyroid hormone or retinoic acid. *The Journal of comparative*
875 *neurology* **522:** 98-117

876
877 Suzuki SC, Bleckert A, Williams PR, Takechi M, Kawamura S, Wong RO (2013) Cone
878 photoreceptor types in zebrafish are generated by symmetric terminal divisions of
879 dedicated precursors. *Proceedings of the National Academy of Sciences of the United*
880 *States of America* **110:** 15109-15114

881
882 Tantri A, Vrabec TR, Cu-Unjieng A, Frost A, Annesley WH, Jr., Donoso LA (2004) X-linked
883 retinoschisis: a clinical and molecular genetic review. *Survey of ophthalmology* **49:** 214-
884 230

885
886 Thisse B, Thisse C (2004) Fast release clones: a high throughput expression analysis.
887 *ZFIN Direct Data Submission* **(http://zfin.org)**

888
889 Thisse C, Degrave A, Kryukov GV, Gladyshev VN, Obrecht-Pflumio S, Krol A, Thisse B,
890 Lescure A (2003) Spatial and temporal expression patterns of selenoprotein genes during
891 embryogenesis in zebrafish. *Gene expression patterns : GEP* **3:** 525-532

892
893 Vihtelic TS, Doro CJ, Hyde DR (1999) Cloning and characterization of six zebrafish
894 photoreceptor opsin cDNAs and immunolocalization of their corresponding proteins.
895 *Visual neuroscience* **16:** 571-585

896
897 Walpita CN, Crawford AD, Darras VM (2010) Combined antisense knockdown of type 1
898 and type 2 iodothyronine deiodinases disrupts embryonic development in zebrafish
899 (Danio rerio). *General and comparative endocrinology* **166:** 134-141

900
901 Yokoi H, Yan YL, Miller MR, BreMiller RA, Catchen JM, Johnson EA, Postlethwait JH (2009)
902 Expression profiling of zebrafish sox9 mutants reveals that Sox9 is required for retinal
903 differentiation. *Developmental biology* **329:** 1-15

904

905

906

907 FIGURE LEGENDS
908
909 **Fig. 1** (1.5 column fitting image): Overview of the effects on gene expression in the
910 phototransduction and retinoid recycling pathways with every component shown in the figure
911 representing a transcript that was downregulated following KD of D1+D2 and/or following
912 KD of D3b.
913 The receptor, an opsin (Ops) containing the chromophore 11-cis-retinal, is excited by a
914 photon, converting the chromophore to all-trans-retinal. Transducin (T), a regulatory G
915 protein bound to opsin, dissociates into Tα and Tβγ. Tα binds to the γ-subunits of
916 phosphodiesterase (PDE) and activates this enzyme. The Tβγ-subunit associates with
917 phosducin (PD), inhibiting re-association with Tα, thereby increasing the duration of visual
918 excitation. PDE breaks down cGMP into 5'-GMP, leading to a decrease of the cGMP
919 concentration. This causes hyperpolarisation, and a decreased Ca^{2+} concentration, by closing
920 of Na^{+}/Ca^{2+} channels. Hyperpolarisation results in an excitatory signal down the neural
921 pathway. At low Ca^{2+} concentrations, calcium binding protein (CaBP) binds to guanylate
922 cyclase (GC). GC converts GTP to cGMP, restoring initial conditions. The regulator of G
923 protein signaling (RGS), an isomerohydrolase, returns Tα to its original state. Ops is
924 phosphorylated by rhodopsin kinase (RK), bound to recoverin (Recov). Arrestin (Arr) then
925 binds the inactivated Ops and facilitates reassociation with Tα and Tβγ. All-trans-retinal is
926 released and reduced to all-trans-retinol, which is transported by retinol binding protein (RBP)
927 to the retinal epithelium where it is converted back to 11-cis-retinal by lecithin retinol
928 acyltransferase (LRAT) and retinal pigment epithelium-specific 65 kDa protein (RPE65).
929
930 **Fig. 2** (2 column fitting image): Heat map of differentially expressed transcripts regarding
931 neurotransmitters and eye development. Green indicates downregulated (Log2FC $\leq$ -0.585,
932 FDR $\leq$ 0.05), and red indicates upregulated (Log2FC $\geq$ 0.585, FDR $\leq$ 0.05) transcripts. White
933 boxes indicate that transcripts were not differentially expressed. D1D2MO: KD of D1+D2;
934 D3bMO: KD of D3b.
935
936 **Fig. 3** (1 column fitting image): In situ hybridization of *dio2* and *dio3b* on consecutive
937 transverse cryosections of the eye of uninjected control zebrafish at 3 dpf. (A) *dio2* AS: *dio2*
938 is expressed throughout all layers of the retina and most strongly in the OPL and ONL. (B)
939 *dio2* S: negative control. (C) *dio3b* AS: *dio3b* is also expressed in all retinal layers. (D) *dio3b*
940 S: negative control. The different layers of the retina are indicated as GCL: ganglion cell
941 layer; IPL: inner plexiform layer; INL: inner nuclear layer; OPL: outer plexiform layer; ONL:
942 outer nuclear layer. AS: antisense probe; S: sense probe.
943
944 **Fig. 4** (1 column fitting image): Effects of deiodinase KD on morphometric parameters. (A)
945 Eye size at 29 hpf, 4 and 7 dpf. (B) Body length at 29 hpf, 4 and 7 dpf. (C) Calculated relative
946 eye size (RES) values (observed eye size divided by expected eye size, see supplementary
947 Fig. S2) at 4 and 7 dpf. Data represent mean + SEM ($n \geq 47$ per group). Statistical significance
948 scores are based on coefficients of a mixed effects model (batch=random effect). ** $p<0.01$,
949 *** $p<0.001$. SCMO: control group, D1D2MO: KD of D1+D2; D3bMO: KD of D3b.
950
951 **Fig. 5** (1.5 column fitting image): Effects of deiodinase KD on retinal lamination.
952 Hematoxylin and eosin stain on cross sections of the eye of control and KD animals at 3 and 7
953 dpf. The different layers of the retina are denoted in the control conditions. GCL: ganglion
954 cell layer; IPL: inner plexiform layer; INL: inner nuclear layer; OPL: outer plexiform layer;
955 ONL: outer nuclear layer. SCMO: control group, D1D2MO: KD of D1+D2; D3bMO: KD of
956 D3b.

Fig. 6 (2 column fitting image): Effects of deiodinase KD on relative rod and cone photoreceptor number. (A-L) Immunohistochemical stainings with Zpr3, Zpr1, anti-blue opsin and anti-UV opsin antibodies on cryosections of the eye of control (A,D,G,J), D1D2MO (B,E,H,K) and D3bMO (C,F,I,L) larvae at 3 dpf. Zpr1 is a marker for both green and red cone photoreceptors, Zpr3 is a marker for rod photoreceptors and anti-blue and anti-UV opsin label the outer segment of blue and UV cone photoreceptors respectively. Blue: DAPI staining of the nuclei; Green: Zpr1/Zpr3+Alexa488 or anti-blue/anti-UV+FITC. (M-P) Data for relative rod/cone number (expressed per retinal surface area) are shown as mean + SEM ($n \geq 5$ per group). Groups with no common letter are significantly different ($p<0.05$). Data in (N,O,P) followed Gaussian distribution and were analyzed by one-way ANOVA with Tukey post hoc test. Data in (M) did not assume Gaussian distribution and were analyzed by Kruskal-Wallis and Dunn's post hoc test. SCMO: control group, D1D2MO: KD of D1+D2; D3bMO: KD of D3b.

Fig. 7 (1 column fitting image): Optokinetic response test to reveal visual impairments. Semi-quantitative scoring of the optokinetic response (OKR) test at 100 hpf and 7 dpf for control, KD and rescue larvae. Data show a significant delay for D3bMO when compared to control and D1D2MO larvae at 100 hpf and compared to all groups at 7 dpf ($p<0.001$ and $p<0.05$ respectively, Chi-square statistics). Co-injection with hD3 mRNA partially rescues the phenotype. SCMO: control group, D1D2MO: KD of D1+D2; D3bMO: KD of D3b, D3bMO+hD3 RNA: rescue group; Full OKR: normal optokinetic response with the eyes following the movement of the stripes and returning to their original position; Partial OKR: the eyes follow the movement of the stripes but do not return to their original position after reaching the border of the visual field; no OKR: fish do not respond to the moving stripes.

Fig. 8 (1 column fitting image): Analysis of the light response in control and deiodinase KD larvae. The light response was analyzed at 4 dpf (A,B), 5 dpf (C,D) and 7 dpf (E,F). The left column depicts average activity patterns for the different conditions throughout the test period. The right column specifically compares activity in the last 2 min in the dark with activity during the first 10 s of light. Boxes show median with 25th and 75th percentiles. Whiskers represent 10th and 90th percentiles. Statistical comparisons were made using wilcoxon-matched pairs signed rank test. *: significant difference between activity in dark and light, i.e. significant light response ($p<0.05$). SCMO: control group, D1D2MO: KD of D1+D2; D3bMO: KD of D3b.

Supplementary Fig. S1: Heat map of differentially expressed transcripts in phototransduction and retinoid recycling pathways. Green indicates downregulated ($Log2FC \leq -0.585$, $FDR \leq 0.05$), and red indicates upregulated ($Log2FC \geq 0.585$, $FDR \leq 0.05$) transcripts. White boxes indicate that transcripts were not differentially expressed. D1D2MO: KD of D1+D2; D3bMO: KD of D3b.

Supplementary Fig. S2: Eye growth in function of body length. (A) Exponential relationship between eye size (μm^2) and body length (μm) for uninjected control embryos between 20-47 hpf. (B) Linear regression model (eye size in function of body length) for uninjected control larvae of 3, 4, 5 and 7 dpf. The equation, R^2 value and p value are shown in the graph.

Figure 1

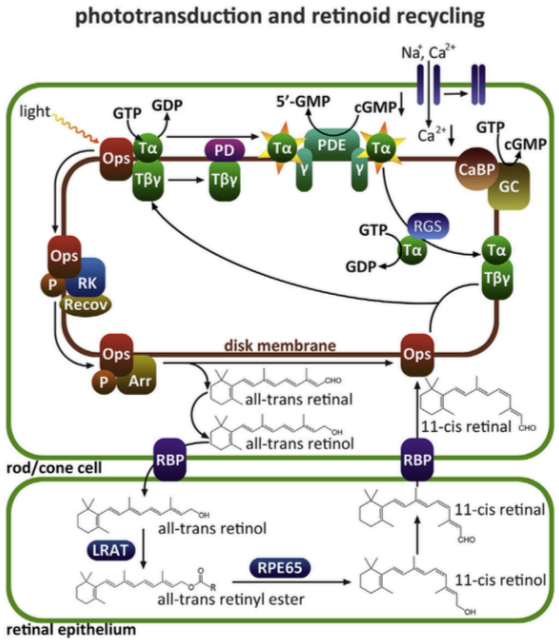

Figure 2

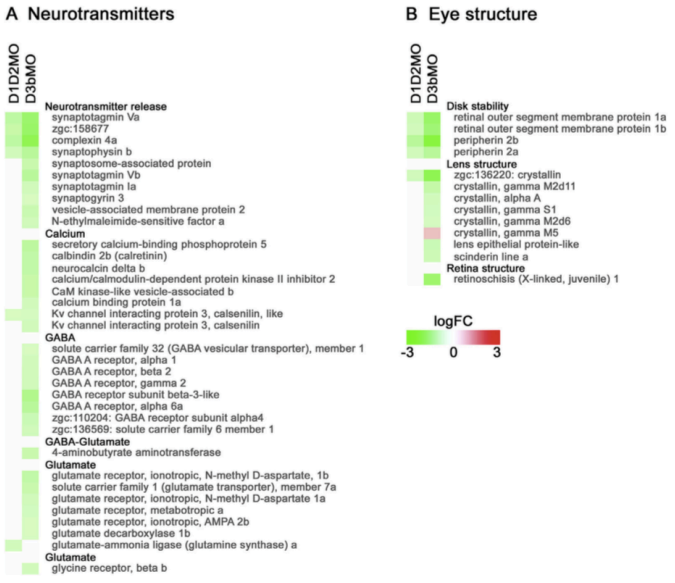

Figure 3

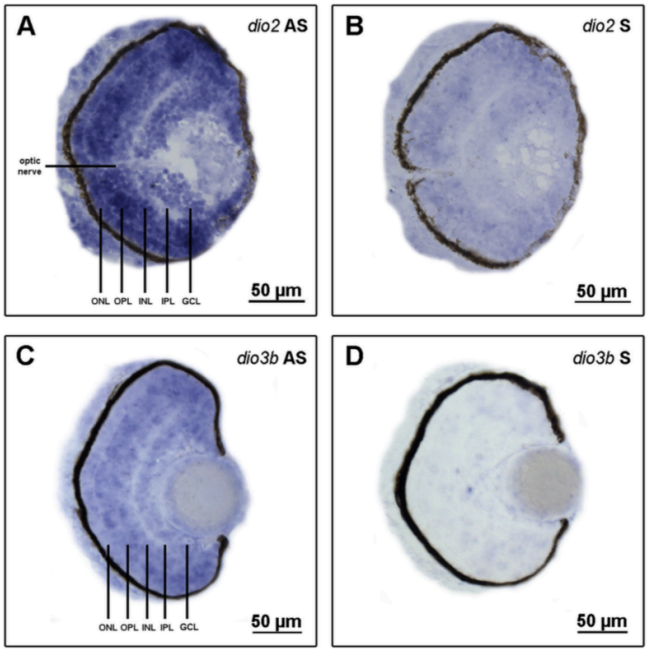

Figure 4

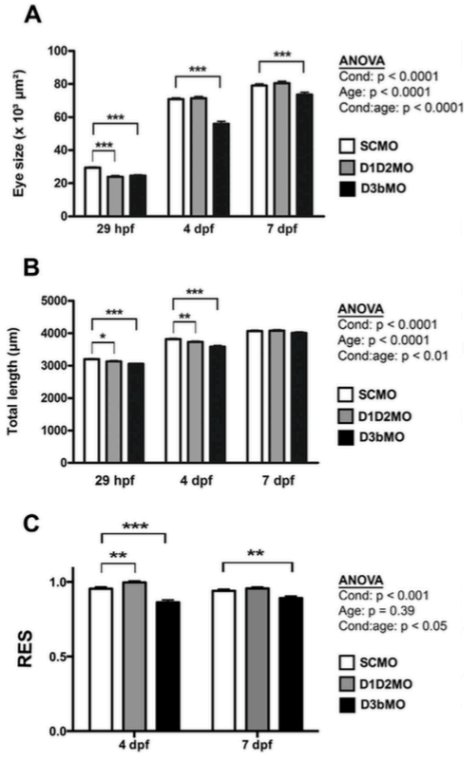

Figure 5

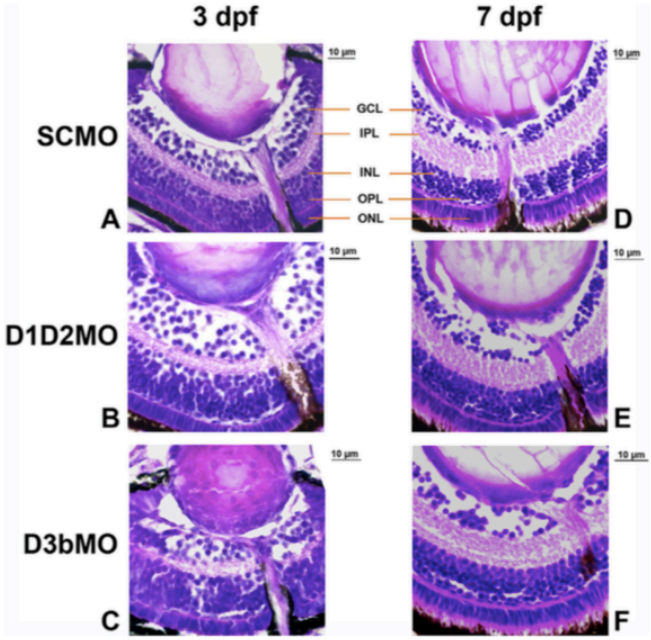

Figure 6

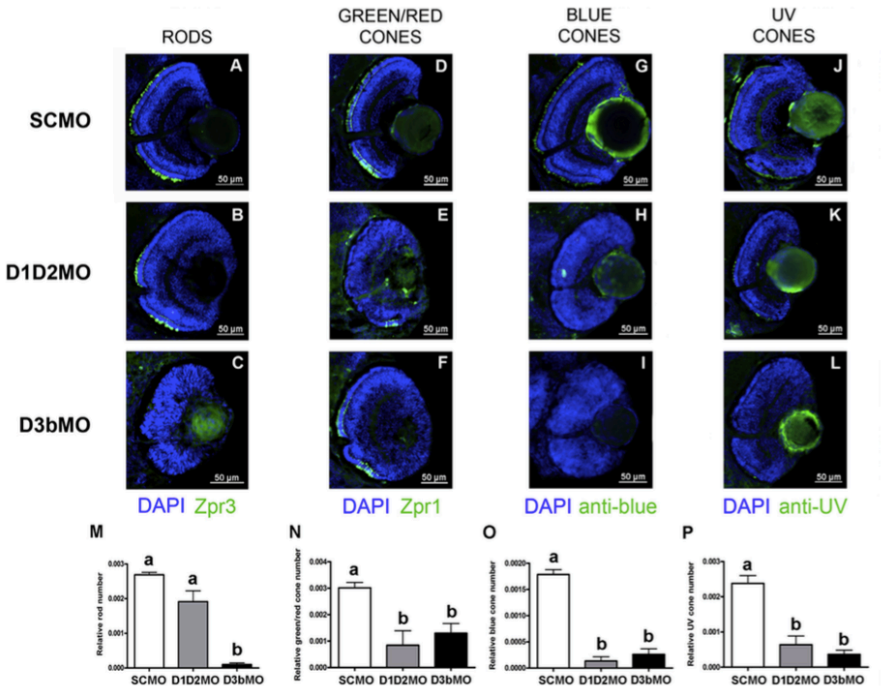

1029 Figure 7

1030

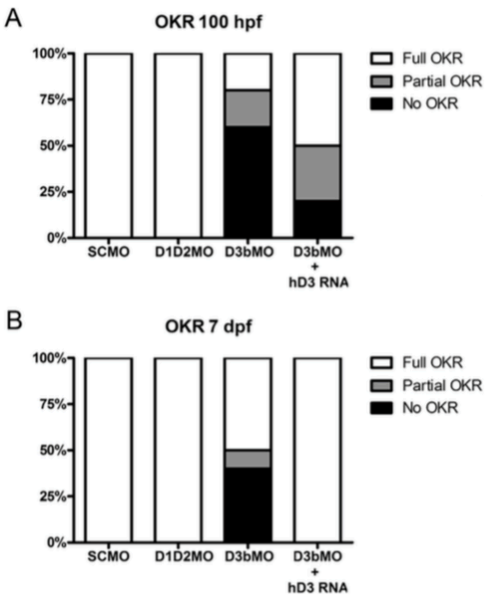

1031

1032 Table 1: Summary of the replicates for the different morphological and functional analyses

	Experiment	Number of batches	Number of animals per condition in each batch
1	Q-PCR	3	20
2	Morphometric analysis	3	n=14-22
3	Retinal morphology	2	n=3
4	Rod photoreceptor counting	1	n=11-16
5	Cone photoreceptor counting (2 stages)	2	n=11-15
6	Cone photoreceptor counting (3 stages)	1	n=5-17
7	Optokinetic response	5	n=10
8	Light response	2	n=48

1033
1034
1035

Table 2: Deiodinase enzyme activity in D1D2MO and D3bMO zebrafish at 3 and 7 dpf

D1+D2 KD	**SCMO**		**D1D2MO**	
	1 nM T_4	**100 nM T_4**	**1 nM T_4**	**100 nM T_4**
3 dpf	0.236±0.012	16.16±1.01	0.021±0.002 9.0%	3.52±0.87 21.8%
7 dpf	0.282±0.002	24.76±0.91	0.162±0.028 57.3%	15.85±0.89 64.0%
D3b KD	**SCMO**		**D3bMO**	
	1 nM T_3		**1 nM T_3**	
3 dpf	0.685±0.014		0.047±0.047 6.9%	
7 dpf	0.769±0.033		0.381±0.036 49.6%	

Enzyme activities are expressed as the amount T_4 or T_3 deiodinated/mg protein/min. Substrate concentrations of 1 nM T_4 and 100 nM T_4 are representative for D2 and D1 activity respectively. Values represent mean ± SEM (n=3). Activity percentages in D1D2MO larvae are also expressed relative to the mean of control, age-matched larvae (SCMO).
The results for D1+D2 KD and D3b KD were obtained in separate experiments.

Table 3: Eye-specific changes in gene expression in D1D2MO and D3bMO zebrafish at 3 dpf

Gene	D1D2MO	D3bMO
rho	-3.00±0.36	-2.79±0.23
opn1sw1	-3.36±0.56	-2.99±0.23
opn1sw2	-3.03±0.3	-2.39±0.19
opn1mw1	-3.68±0.54	-3.17±0.22
opn1lw2	-2.92±0.40	-2.22±0.17
pde6h	-2.79±0.59	-2.32±0.09
pde6a	-2.18±0.16	-1.89±0.07
grk1b	-2.83±0.51	-2.79±0.20
arr3a	-2.52±0.29	-2.07±0.20
rpe65a	-1.28±0.14	-1.11±0.09

10 genes were selected from the microarray results to represent the excitation and recovery pathway. 4 biological replicates (each one containing 40 eyes) were used per condition. Values for D1D2MO (KD of D1+D2) and D3bMO (KD of D3b) represent mean ± SEM for the log2 fold change relative to the average expression in SCMO-injected (control) larvae.

Table 4: Relative rod and cone photoreceptor number in D1D2MO and D3bMO zebrafish at 4 and 7 dpf

	SCMO	D1D2MO	D3bMO
4 dpf			
Green + red cones	3.48±0.10 [a]	3.16±0.20 [ab]	2.84±0.19 [b]
Blue cones	2.12±0.13 [a]	1.89±0.16 [ab]	1.61±0.14 [b]
UV cones	2.72±0.13 [a]	3.16±0.16 [a]	1.64±0.19 [b]
Rods	3.17±0.08 [a]	3.00±0.12 [a]	2.80±0.14 [a]
7 dpf			
Green + red cones	2.83±0.15 [a]	2.49±0.17 [a]	2.49±0.09 [a]
Blue cones	2.19±0.10 [a]	1.88±0.11 [a]	2.16±0.09 [a]
UV cones	2.37±0.15 [a]	2.51±0.10 [a]	2.17±0.21 [a]

Data represent relative cone/rod numbers per retinal surface area (expressed as number x 10^{-3}/pixel²) and are shown as mean ± SEM ($n \geq 5$ per group). The following antibodies were used: Zpr1 (green and red cones), anti-blue opsin (blue cones), anti-UV opsin (UV cones) and Zpr3 (rods). Rod data were obtained in a separate experiment and only counted at 4 dpf. For a given opsin and stage groups with no common letter are significantly different ($p<0.05$). Data followed Gaussian distribution and were analyzed by one-way ANOVA with Tukey post hoc test.

Supplementary Table S1: 10 candidate genes for Q-PCR analysis with corresponding primer pairs

Gene	Forward primer	Reverse primer	Acc Nr.	Amplicon length	Source
rho	ACTTCCGTTTCGGGGAGAAC	GAAGGACTCGTTGTTGACAC	NM_131084	176	(Laranjeiro & Whitmore, 2014)
opn1sw1	TTCCAAAGTCAGCCCCTTCG	GTTCATAGGTGTGCCCACGA	NM_131319	112	(Laranjeiro & Whitmore, 2014)
opn1sw2	TAACCTCATTCTGCGGACGAACCA	CATGTTCAGCAAGCCAAGACCAAG	NM_131192	141	(Krishnan et al, 2008)
opn1mw1	ACACCCTTTTCTGTGGCAAG	ATGACGGAGCACTGAATAGGC	NM_131253	120	(Laranjeiro & Whitmore, 2014)
opn1lw2	CACAATCAGCGTCATCAATC	AGTCCAGCAATACCACATAC	NM_001002443	102	IDT primer design
pde6a	CAGTCAACAAGATCGGGGCT	GCTCAGGTGAAACACTCGGA	NM_001007160	104	(Laranjeiro & Whitmore, 2014)
pde6h	AGAGAGGAGGACCACCAAAGT	CCATTCCTGGGATGTCGTCT	NM_200785	105	(Laranjeiro & Whitmore, 2014)
grk1b	ATCGAGAAGCGAATCCTGGC	GCAAATGCTCAAGCCCACAA	NM_001017711	217	(Liu et al, 2015)
arr3a	TGGTATCAGGCGGAGGTCTG	TTCTTCTGCCGTCTCGCTGT	NM_001002405	176	(Rey et al, 2013)
rpe65a	GCCCCGCAGCCAGAAGTCAG	ACGAGTCGGGCTCCTGCCAT	NM_200751	319	(Higdon et al, 2013)
actb1	AAGTGCGACGTGGACA	GTTTAGGTTGGTCGTTCGTTTGA	NM_131031	341	(Gonzalez et al, 2006)
eef1a1l1	TGTCCTCAAGCCTGGTAT	CATTACCACGACGGATGT	NM_131263	164	IDT primer design

We selected 10 genes to represent the excitation and recovery pathway. The two housekeeping genes were *act1b* and *eef1a1l1*. Each gene is shown with its primer pair, accession number, amplicon length and reference source. Description of all genes: *opn1sw1*, opsin 1 (cone pigments), short-wave-sensitive, 1 (UV); *opn1sw2*, opsin 1 (cone pigments), short-wave-sensitive, 2 (blue); *rho*, rhodopsin; *opn1mw1*, opsin 1 (cone pigments), medium-wave-sensitive, 1 (green); *opn1lw2*, opsin 1 (cone pigments), long-wave-sensitive, 2 (red); *pde6a*, phosphodiesterase 6A, cGMP-specific, rod, alpha; *pde6h*, phosphodiesterase 6H, cGMP-specific, cone, gamma; *grk1b*, G-protein coupled receptor kinase 1 b (cone); *arr3a*, arrestin 3a; *rpe65a*, retinal pigment epithelium-specific protein 65a; *actb1*, actin beta1; *eef1a1l1*, eukaryotic translation elongation factor 1 alpha 1, like 1.